**Highlighting collaborative research from Professors Antonio Frontera and Emanuele Priola, this study stems from the Chemistry Departments of the University of the Balearic Islands in Spain and the University of Torino in Italy.**

Synthesis, X-ray characterization and DFT analysis of dicyanidoaurate telluronium salts: on the importance of charge assisted chalcogen bonds

This study presents the synthesis and X-ray characterization of two cyanidoaurate telluronium salts. In both, the tellurium atom forms three directional chalcogen bonds (ChBs) with neighboring anions. Using DFT and several computational tools, the presence of three σ-holes at the Te-atoms was identified, facilitating strong charge-assisted ChBs with counter-ions. Additionally, notable charge transfer from the anion's N-atom lone pair to the cation's σ*(Te–C) orbital is observed.
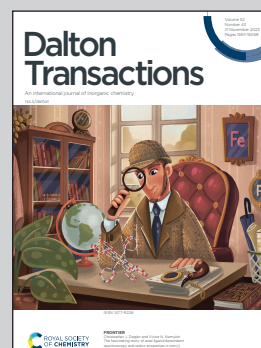
ROYAL SOCIETY
OF **CHEMISTRY**

rsc.li/dalton

Check for updates

Synthesis, X-ray characterization and DFT analysis of dicyanidoaurate telluronium salts: on the importance of charge assisted chalcogen bonds†

Simone Ghinato,[a] Alessia Giordana, [ID] *[a] Eliano Diana, [ID] [a] Rosa M. Gomila, [ID] [b] Emanuele Priola [ID] *[a] and Antonio Frontera [ID] *[b]

In this manuscript we report the synthesis and X-ray characterization of two cyanidoaurate telluronium salts, namely (3-fluorophenyl)(methyl)(phenyl)telluronium dicyanidoaurate [(3-F-Ph)(Me)(Ph)Te][Au(CN)$_2$] (**1**) and methyldiphenyltelluronium dicyanidoaurate [(Me)(Ph)$_2$Te][Au(CN)$_2$] (**2**). In the solid state, the tellurium atom establishes three concurrent and directional chalcogen bonds (ChBs) with the adjacent anions, in both compounds. These charge-assisted ChBs (CAChBs) have been analyzed using DFT calculations and several computational tools. The MEP surface analysis discloses the existence of three σ-holes at the Te-atoms capable of establishing strong CAChBs with the counter-ions. In addition, significant charge transfer from the lone pair orbital at the N-atom of the anion to the antibonding σ*(Te−C) orbital of the cation is observed in some cases.

Introduction

Organotelluronium salts are interesting compounds with applications as reactants in organic synthetic chemistry. In particular, they are precursors of telluronium ylides that can react with carbonyl compounds to yield oxiranes and secondary alcohols.[1] These compounds have been known for over a century[2] and their solid state architecture[3–14] was described as being governed by tellurium–anion interactions.[15] They were classified as secondary weak interactions that expanded the TeR$_3$E (E = lone pair) trigonal pyramidal geometry into a five- or six-coordinate entity.[16,17] Solid-state [125]Te-NMR spectroscopy was also used as a sensitive tool for the identification of these weak secondary bonding interactions between the cations and anions.[13]

More recently, noncovalent interactions involving elements of the p-block of the periodic table, in general behaving as electrophiles, have been attracting considerable attention.[18–23] Several theoretical[24] and experimental[25] works have demonstrated that the electron density distribution in the covalently

bonded atoms of p-block is anisotropic and shows regions of lower (positive) or higher (negative) electron density. The location and number of positive regions are related to the position and number of covalent bonds formed by the atoms.[26] For instance, chalcogen atoms typically form two covalent bonds and, consequently, two regions of depleted electron density (named σ-holes) are usually located opposite these bonds.[27] With electron-rich sites, these σ-holes form highly directional interactions which are named chalcogen bonds (ChBs).[28] Similar names are used for interactions involving elements of groups 17 and 15: halogen bonds (HaBs),[18] and pnictogen bonds (PnBs),[20,29] respectively.

Interest in ChB has increased exponentially in the last ten years.[19,30–32] It has been recently used in catalysis,[33,34] molecular recognition, and crystal engineering.[35] More recently, the utilization of trivalent sulfur cations as ChB donor sites (R$_3$S$^+$···A) has been studied both theoretically and experimentally.[36–38] Trisubstituted sulfur atoms afforded charge-assisted chalcogen bonds (CAChBs), which are particularly strong thanks to the contribution of the cation–anion electrostatic attraction. Moreover, the existence of three σ-holes in the chalcogen atom enables the possibility of establishing up to three ChBs.[36–38] In this regard, Resnati *et al.*[36] have demonstrated the existence and relevance of CAChBs in crystal structures and enzyme inhibitors of α-glucosidase and analyzed the energetic features of supramolecular assemblies of sulfonium, selenonium and telluronium salts. In these systems, the Ch-atoms possess three σ-holes available to interact with electron rich atoms, mimicking the behavior of pnictogen bonds.

aUniversità degli Studi di Torino, Department of Chemistry, Via Pietro Giuria 7, 10125 Torino, Italy. E-mail: alessia.giordana@unito.it, emanuele.priola@unito.it
bDepartment of Chemistry, Universitat de les Illes Balears, Crta de Valldemossa km 7.5, 07122 Palma de Mallorca, Baleares, Spain. E-mail: toni.frontera@uib.es

X-ray structures of telluronium cations where the counterion contains gold are very rare. To the best of our knowledge, only two examples are available in the literature: one corresponds to triphenyltelluronium with tetrachloridoaurate (refcode MIHSOL)[39] and the other to trimethyltelluronium with bis(4,5-dimercapto-1,3-dithiole-2-thionato)-gold(III) (refcode LALFUZ),[40] with both compounds incorporating Au(III) in a square planar environment, see Scheme 1. In this manuscript, we report for the first time asymmetric telluronium salts including Au(I) dicyanoaurate as a counterion. In particular, we analyze the structure and bonding of (3-fluorophenyl)(methyl)(phenyl)telluronium dicyanidoaurate [[(3-F-Ph)(Me)(Ph)Te][Au(CN)$_2$] **1** and methyldiphenyltelluronium dicyanidoaurate [[(Me)(Ph)$_2$Te][Au(CN)$_2$] **2** and the effect of the geometry on the cation–anion interactions. The assemblies, constructed by chalcogen bonding interactions, have been described and studied using DFT calculations, molecular electrostatic potential (MEP) surface analysis and two computational tools based on the topology of the electron density, QTAIM[41] and NCIPlot.[42] Moreover, the donor–acceptor orbitals involved in the ChBs were analyzed using the natural bond orbital (NBO) methodology[43] and the Kitaura–Morokuma[44] energy decomposition analysis.

Materials and methods

Synthesis of complexes 1 and 2

Compounds **1** and **2** have been obtained by metathesis. Ethanolic solutions of equimolar amounts of K[Au(CN)$_2$] (Merck, used without any purification) and the corresponding tetrafluoroborate salts, **3a** and **3b**, respectively (synthesized and purified as described in Scheme 2 and the ESI†), were mixed and from slow evaporation, few prismatic colorless crystals started to appear after a few weeks. Crystals were separated from the mother solution before the formation of other by-products.

Single-crystal X-ray diffraction

Single crystal data of crystallized compounds were collected on a Gemini R Ultra diffractometer (Agilent Technologies UK Ltd, Oxford, U.K.) using graphite-monochromatic Cu Kα radiation (λ = 1.5406 Å) with the ω-scan method. Copper derived radiation
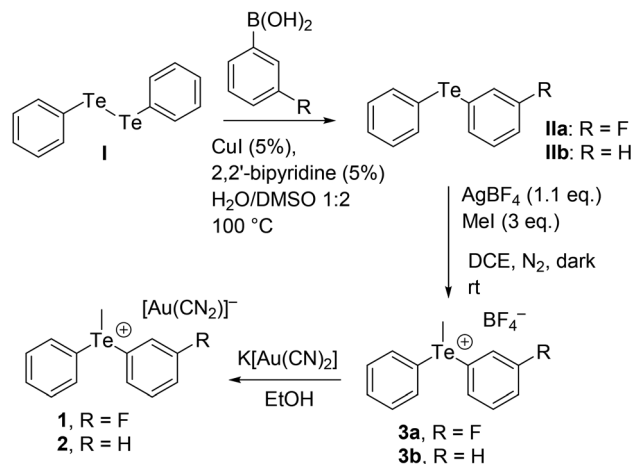
**Scheme 2** Synthetic route to compounds **1–3**.

has been preferred for cases of very weakly diffracting crystals. CrysAlisPro software was used for retrieving cell parameters, performing data reduction and absorption correction (with the multi-scan technique). All structures were solved by direct methods using SHELXS-14 and refined with full-matrix least-squares on F^2 using SHELXL-14 using the Olex^2 program. All non-hydrogen atoms were anisotropically refined. Hydrogen atoms were calculated and refined as riding on the corresponding atom. Images of the structures were obtained using Mercury software. Crystal data and refinement, selected bond lengths and angle amplitudes and the asymmetric units of compounds are reported in the ESI.† The crystallographic data for the crystallized compounds have been deposited at the Cambridge Crystallographic Data Centre as supplementary publications under CCDC numbers 2284002 and 2284003.†

Characterization

FT-ATR spectra were recorded in the 50–4000 cm^{-1} range using a Bruker Vertex 70 spectrophotometer equipped with a Harrick MVP2 ATR cell and DTGS detectors (either with Si or KBr beamsplitters). Micro Raman spectra of single crystals were recorded using a Horiba Jobin Yvon HR800 spectrometer, equipped with an Olympus BX41 microscope, by exciting with a 532 nm laser.

DFT calculations

The energy and EDA calculations were carried out using the Turbomole 7.7 program[45] and the PBE0[46]-D4[47]/def2-TZVP[48] level of theory. For gold, the def2-TZVP basis set used in this work included effective core potentials (ECP),[49] and relativistic effects were used for the inner electrons.[48] The crystallographic coordinates were used to evaluate the interactions in the solid state of compounds **1** and **2**, since we were interested in studying the interactions as they stand in the solid state. The dimers and trimers extracted from the solid-state structures were selected to study the chalcogen bonding interactions. The interaction energies were computed by subtracting the sum of
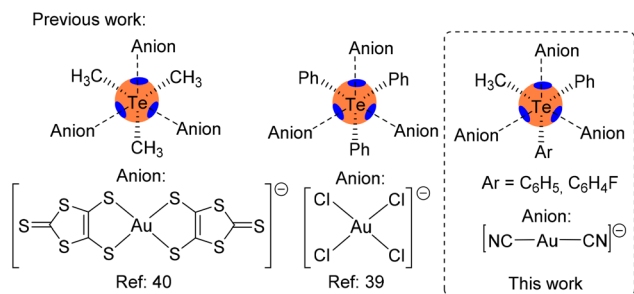
Scheme 1 Left: previous examples of telluronium cations with Au-based anions. Right: the telluronium salts studied herein.

the energies of the monomers from those of the assembly. Bader's "Atoms in molecules" theory (QTAIM)[41] and the non-covalent interaction plot (NCIPlot)[42] were used to study the interactions discussed herein using the Multiwfn program[50] and represented using the VMD visualization software.[51] The molecular electrostatic potential (MEP) surfaces were computed using the 0.001 a.u. isosurface as the best estimation of the van der Waals surface at the same level of theory and represented using the GaussView program.[52] For the NCIPlot representations, the following settings were used: RDG isosurface = 0.4, density cut-off = 0.04 a.u., and color scale $-0.03 \leq$ (signλ_2)$\rho \leq 0.03$ a.u. Natural bond orbital (NBO)[43] calculations were performed using the NBO7.0 program.[53]

Results and discussion

Description of the structures

Both the dicyanidoaurate salts crystallize from ethanol in the monoclinic space group $P2_1/n$ and are isomorphous. Both salts present a crystal packing similar to the dicyanoargentate derivative of the methyldiphenyltelluronium cation (refcode HUHBUH) (Fig. 1).[54]

In both crystal structures (Fig. 2), the telluronium cation forms dimeric nodal chains. These chains are constructed with two bridging dicyanoaurate chalcogen-bonded cyanides and two terminal dicyanidoaurate chalcogen-bonded cyanides, as shown in Fig. 2b for compound **2**. These interactions constitute the secondary coordination sphere for the tellurium(IV) centre, as illustrated in Scheme 1 and detailed in Table 1.

Comparative analysis of the distances reveals a noticeable increase in the strength of chalcogen bonding (ChB) upon the introduction of a fluorine substituent, as presented in Table 1. Notably, no metallophilic interactions are discerned in structures **1** and **2**. However, a robust argentophilic interaction is prominent in HUHBUH (with distances of $d(Au1\cdots Au1) =$ 3.7970(4) Å in **1**, $d(Au1\cdots Au1) = 3.9272(4)$ Å in **2**, and $d(Ag1\cdots Ag2) = 3.171(2)$ Å in HUHBUH). This observation suggests that while ChB is consistently present, it exhibits greater directionality within dicyanoaurate compared to dicyanoargentate. In the latter case, the transition towards argentophilicity is more feasible, albeit typically less energetically favourable than in the case of gold. This underscores the importance of interaction directionality and appropriate coun-
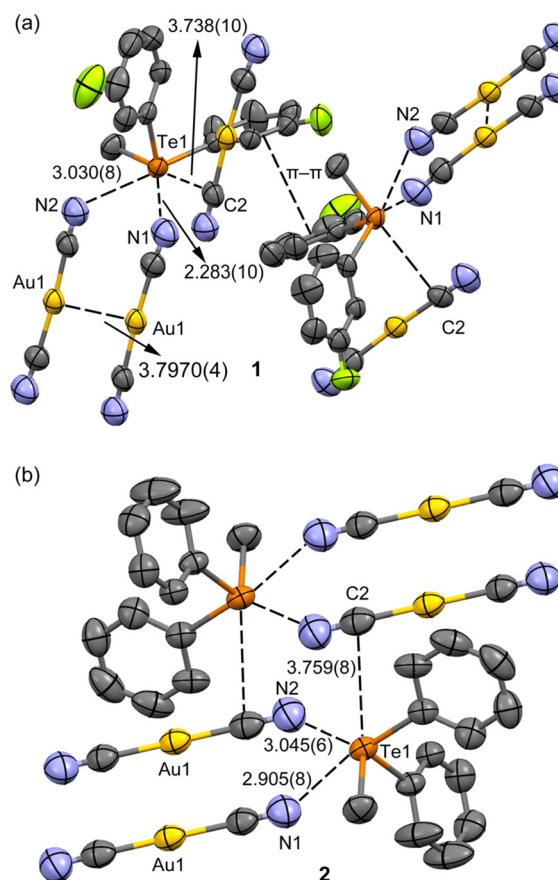

Fig. 2 (a) Details of the ChBs and π···π stacking interactions in **1** and (b) the dimeric motif in **2**. Distances in Å. Geometric features of the π-stacking: Cg···Cg distance: 4.026 Å, and angles between ring planes: 9.87°.

Table 1 Chalcogen bond lengths ($d_{Ch\cdots A}$) and angles between tellurium and the cyano groups in the crystal packing. The $\delta_{Ch\cdots A}$ values (%) and the classification of the ChBs are indicated

Cmpnd	ChB[a]	$d_{Ch\cdots A}$ (Å)	Angle (°)	$\delta_{Ch\cdots A}$[b]	Strength[c]
1	C10−Te1···N1[i]	2.873(10)	170.8(3)	−20.4	m–s
1	C4−Te1···N2[ii]	3.030(8)	169.4(3)	−16.1	w
1	C3−Te1···C2[i]	3.738(10)	164.5(3)	−0.6	w
2	C10−Te1···N1[i]	2.905(8)	170.9(2)	−19.5	m–s
2	C4−Te1···N2[iii]	3.045(6)	170.8(2)	−15.7	w
2	C3−Te1···C2	3.759(8)	164.3(2)	0.0	w

[a] i = $-1 + x$, y, and z; ii = $1 - x$, $-y$, and $1 - z$; iii = $-x$, $2 - y$, and $-z$. [b] $\delta_{Ch\cdots A} = \{[d_{Ch\cdots A}-(r_{vdWCh} + r_{vdWA})]/(r_{vdWCh} + r_{vdWA})\}\cdot 100$. [c] m: medium; s: strong; w: weak.
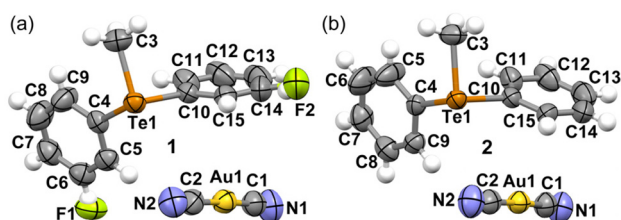

Fig. 1 Ellipsoid plots (50% probability) of the asymmetric units of salts **1** (a) and **2** (b).

terion geometry in establishing robust metallophilic interactions.[55]

The $\delta_{Ch\cdots A}$ values for the Te···N and Te···C chalcogen bonding interactions in compounds **1** and **2** were derived using the equation proposed by Aragoni *et al.*[56] and are given in Table 1. These values shed light on the relative shortening

of the ChB distances compared to the sum of the involved vdW radii and also offer a reference against average values obtained from the CSD. A ChB strength scale, based on these $\delta_{Ch\cdots A}$ values, has been suggested in ref. 56. Analysing the $\delta_{Ch\cdots A}$ values from Table 1 and referencing the literature scale,[56] we deduce that both compounds presented feature one medium-strong ChB (Te1⋯N1 contact) and two weaker interactions (Te1⋯N2 and Te1⋯C2).

Upon examining the arrangement of aromatic rings, an intriguing observation emerged: the fluoro derivative displayed a shifted π⋯π stacking interaction (Fig. 2a) absent in the unsubstituted salt. This particular stacking interaction could be attributed to dipolar forces stemming from the asymmetrically charged phenyl groups of the telluronium cation. Furthermore, it is noteworthy that in both cases, the dicyanoaurate did not participate in the classical Au⋯π interactions. This characteristic is intriguing, considering that the coulombic component aligns with certain previously studied systems.[57] These findings emphasize the pivotal role of ChBs in shaping the X-ray packing of both structures, complemented by directional anion⋯π interactions explored in the subsequent sections.

Table 2 shows a compilation of the geometric characteristics of the ChBs in other asymmetric telluronium salts sourced from the Cambridge Structural Database (CSD). Broadly speaking, these distances align well with those in Table 1 for compounds **1** and **2** discussed in this study. Additionally, the Te⋯μ-CN distances in compounds **1** and **2** show strong consistency with the Te⋯π(C_6H_5) distances in the CSD refcode LOXPOD, where the ChBs form between the Te atom and the π-system of the aromatic rings.

Spectroscopic characterization

Infrared and Raman spectra of **1**, **2** and their tetrafluoroborate salt precursors ([(3-F-Ph)(Me)(Ph)Te](BF_4) (**3a**) and [(Me)(Ph)$_2$Te](BF_4) (**3b**)) were recorded on solid samples and the vibrational frequencies and assignment are listed in Table S7, ESI.†

Table 2 Chalcogen bond lengths between asymmetric tellurium cations and anions in structures retrieved from the CSD

CSD reference	Anion	Lengths (Å)
GUNVIX	BF_4^-	3.138–3.287
IXOMUG	BF_4^-	2.871–3.263
JOMQIL	Cl^-	3.237–3.317
LOXPOD	$B(C_6H_5)_4^-$	3.575–3.750
OHIRON	RSO_3^-	2.840–3.013
POXGAK	Cl^-	3.151
QOBXEK	Br^-	3.633
REQNAY/REQNOM	$CF_3SO_3^-$	2.895–3.101
REQPOO/REQPUU	$CF_3SO_3^-$	2.872–3.029
TAJJAP	ClO_4^-	3.331–3.558
TIZVAZ	RSO_3^-	2.877–3.051
XUPWUB	p-MePhSO$_3^-$	2.815–2.945
YODVUK/YODWEB	I^-	3.347–3.655
YODWAR/YODWIZ	I^-/I_3^-	3.502–3.991

The infrared spectra of crystalline [(Ph)$_2$(Me)Te]I have been reported,[58] and are substantially similar to those of **3b**. The vibrational modes of Te–C have been assigned by comparison with the vibrational spectra of Ph$_2$TeAlg$_2$.[59] The vibrational mode of **3a** has been assigned by comparison with that of **3b** and the vibrational frequencies of fluorobenzene.[60] The vibrational frequencies of telluronium cations **3a** and **3b** seem quite insensitive to the change of BF_4^- with [Au(CN)$_2$]$^-$. A similar behavior is found in [Au(CN)$_2$]$^-$, which has vibrational frequencies very similar to those of the crystalline K[Au(CN)$_2$] salt.[61] Only one vibrational mode seems sensible to the intermolecular interaction between Te and the cyanide group: the stretching of the Te–CH$_3$ bond that undergoes a lowering of nearly 5 cm^{-1} by moving from BF_4^- to the [Au(CN)$_2$]$^-$ anion, which suggests a lowering of the Te–C bond order in consequence of the interaction with a nitrogen lone pair donor.

DFT calculations

To begin, the computation of molecular electrostatic potential (MEP) surfaces for both salts was undertaken to investigate the presence and strength of σ-holes centred on the Te-atoms. To model the salts, the dicyanidoaurate anion closest to the cation, yet not interacting with the σ-holes, was employed. This choice ensured the use of neutral systems, facilitating an accurate analysis of the relative σ-hole intensities. The MEP surfaces are illustrated in Fig. 3 (left), revealing that the MEP minima for both compounds are situated at the N-atom of the cyanido ligand (−63.4 kcal mol^{-1} and −64.0 kcal mol^{-1} for **1** and **2**, respectively).

For a detailed representation of the σ-holes and the electron density anisotropy at the Te-atom, a distinct scale was applied to portray a section of the MEP surface encompassing the
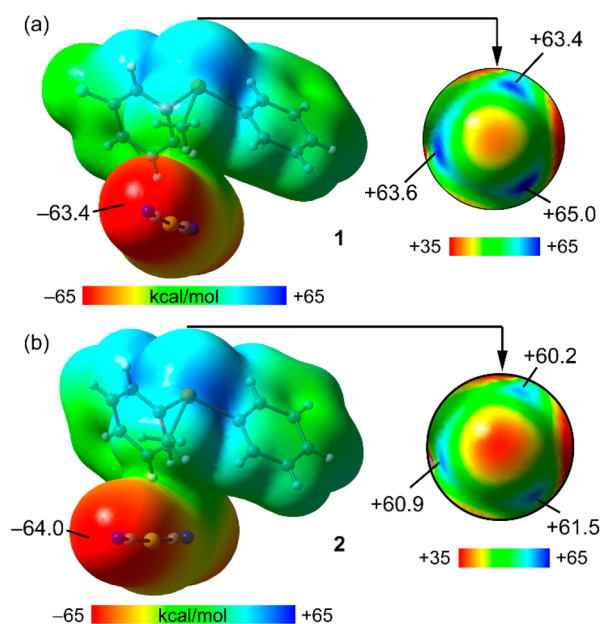

Fig. 3 MEP surfaces (isovalue, 0.001 a.u.) of compounds **1** (a) and **2** (b). Values at selected points are indicated in kcal mol^{-1}.

Te-atom in Fig. 3 (right). Consequently, three distinct σ-holes emerged, positioned on the extension of the three Te–C covalent bonds. In compound **1**, the MEP maximum was positioned at the σ-hole corresponding to the 3-fluorophenyl ring (+65.0 kcal mol^{-1}), while the other two σ-holes exhibited closely similar and slightly lower MEP values (+63.4 kcal mol^{-1} and +63.6 kcal mol^{-1}). This configuration establishes all three σ-holes as favourable sites for interactions with counterions.

In compound **2**, the MEP values at the three σ-holes were comparable, ranging from +60.2 kcal mol^{-1} to +61.5 kcal mol^{-1}, modestly lower when contrasted with those of compound **1**.

As elucidated in the preceding sections, each telluronium cation forms three charge-assisted chalcogen bonds (CAChBs) with dicyanidoaurate anions. The energetic attributes of these CAChBs were individually investigated using DFT calculations and QTAIM/NCIPlot analysis. For energy calculations, the entire salt was treated as a unified entity, and its interaction with an additional anion was computed. For example, in compound **1**, the association [(3-F-Ph)(Me)(Ph)Te][Au(CN)$_2$] + [Au(CN)$_2$]$^-$ was evaluated to yield [(Me)(Ph)$_2$Te][Au(CN)$_2$]···[Au(CN)$_2$]$^-$ for each ChB (referred to as dimers A–C in Fig. 4, as discussed below).

Fig. 4 showcases comprehensive QTAIM/NCIPlot analyses for the three ChB assemblies within compound **1**. Employing both methods in tandem allows for a spatial representation of interactions, discerning their attractive or repulsive nature. In our NCIPlot illustrations, blue signifies potent and attractive interactions, while green denotes weaker and attractive inter-

actions. As depicted in Fig. 4, within all the three studied dimers (A–C), the ChB interaction is defined by a bond critical point (BCP, marked by a red sphere) and a bond path (highlighted by an orange line) linking the N-atom of the anion to the Te-atom of the cation, thus affirming the existence of these three ChBs.

Furthermore, isosurfaces of the reduced density gradient (RDG) manifest coinciding with the BCP positions upon complexation. Notably, the coloration of the RDG isosurfaces differs: green (indicative of weak interactions) for dimer A, dark blue (signifying strong interactions) for dimer B, and a moderately strong bluish hue for dimer C, consistent with the experimental distances. In congruence with the intensity of the σ-hole opposite the 3-fluorophenyl ring, the binding energies incorporated in Fig. 4 reveal that dimer B possesses the most substantial dimerization energy. This outcome aligns with the RDG isosurface colour and the intensity of the aforementioned σ-hole. The other two dimers display closely similar interaction energies due to additional contacts compensating for the greater ChB strength in dimer C. Particularly noteworthy are a C–H···Au hydrogen bond and an anion–π interaction, each characterized by BCPs and green RDG isosurfaces.

The notable dimerization energies highlighted in Fig. 4 further underscore the pivotal role of the three ChBs in guiding the solid-state structure of compound **1**.

A parallel analysis has been conducted for compound **2**, which is elucidated comprehensively in Fig. 5. The arrangement of bond critical points (BCPs), bond paths, and reduced density gradient (RDG) isosurfaces closely mirrors the descrip-
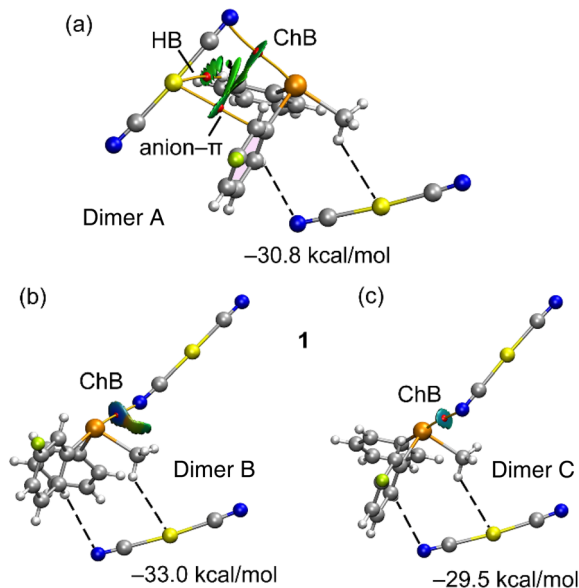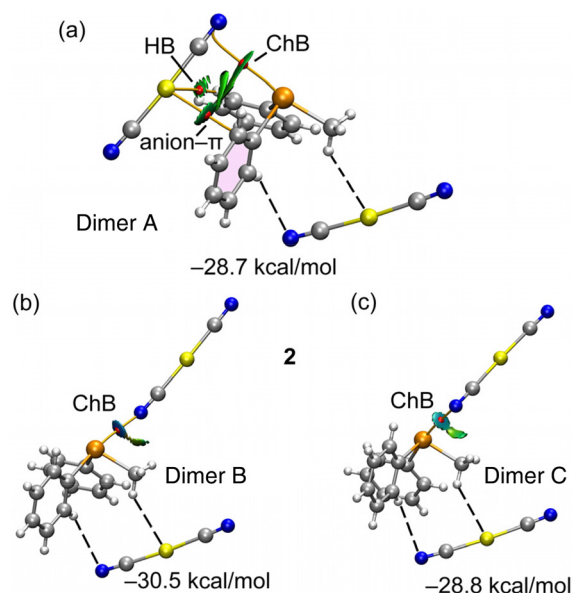

Fig. 4 QTAIM/NCIPlot analysis of ChB dimer A (a) dimer B (b) and dimer C (c) of **1**. Only intermolecular interactions are represented. See theoretical methods for the NCIPlot settings. The dimerization energies are indicated and have been computed considering the telluronium and one [Au(CN)$_2$]$^-$ anion (the one connected with dashed lines) as a monomer.

Fig. 5 QTAIM/NCIPlot analysis of ChB dimer A (a) dimer B (b) and dimer C (c) of **2**. Only intermolecular interactions are represented. See theoretical methods for the NCIPlot settings. The dimerization energies are indicated and have been computed considering the telluronium and one [Au(CN)$_2$]$^-$ anion (the one connected with dashed lines) as a monomer.

tion provided earlier for compound **1**. Remarkably, the dimerization energies are less negative (indicative of weaker interactions) in accordance with the MEP analysis revealing reduced MEP values at the σ-holes within compound **2**. A prominent energy difference of 2.5 kcal mol⁻¹ between the dimers underscores the influence of fluorine substitution on the strength of ChB.

At this juncture, it is insightful to compare the strength of the CAChBs discussed in this study with those documented in the existing literature for neutral ChB donors.[62] While the ChB distances for neutral Te compounds might be comparable or even shorter,[62c] the interaction energies for the CAChBs examined in this study are notably greater due to the supplementary ion-pair effect.

To discern charge transfer effects within the ChB interactions observed in compounds **1** and **2**, NBO analysis was employed. This approach is adept at deciphering donor–acceptor interactions between orbitals and revealing their stabilization energies through second-order perturbation analysis. The summarized outcomes are presented in Table 3. A close review of the results reveals the existence of two distinct orbital donor–acceptor interactions. Both these contributions are shared across compounds **1** and **2**, as well as within the three chalcogen bonding dimers. The primary contribution involves electron donation from a lone pair (LP) orbital of nitrogen, belonging to the Au-coordinated cyanido ligand, to the antibonding σ*(Te–C) orbital, a characteristic trait of σ-hole interactions. A secondary yet less significant contribution emerges from a π-orbital of the C≡N bond to the antibonding σ*(Te–C) orbital.

By evaluating various dimers in this study and considering the second-order orbital energies highlighted in Table 3, it becomes evident that dimer B showcases the most substantial LP(N) → σ*(Te–C) contribution (7.76 kcal mol⁻¹ in **1** and 6.82 kcal mol⁻¹ in **2**). This alignment effectively corresponds to the highest binding energy observed for dimer B and the shortest Te⋯N distances encountered. In addition, it agrees well with the $\delta_{Ch\cdots A}$ values mentioned before (see Table 1). The σ-hole character of the interaction is demonstrated through the analysis of the NBO plots presented in Fig. 6 for dimer B of both compounds. In these plots, the SP-hybridized lone pair originating from one N-atom of the dicyanidoaurate anion
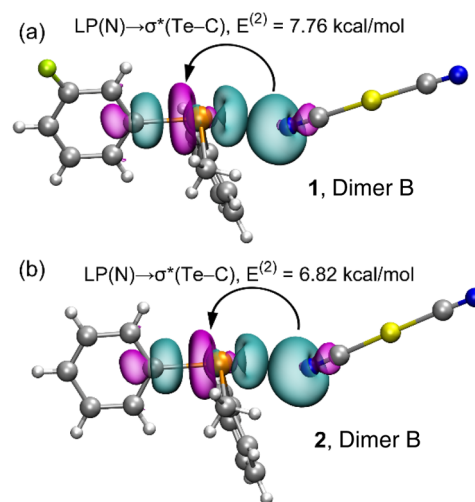

Fig. 6 Plots of the NBOs involved in the electron charge transfer and the associated stabilization energy in the dimer B of compounds **1** (a) and **2** (b).

aligns with the σ*(Te–C) orbital of the telluronium cation in both compounds.

To complement the insights gleaned from the MEP, NBO, and QTAIM/NCIPlot analyses, an energy decomposition analysis (EDA) was undertaken for the three dimers within compound **1**, taken as an illustrative example. The summarized outcomes are presented in Fig. 7, revealing that in all the dimers, the electrostatic contribution takes precedence (indicated by fuchsia bars), followed by the orbital contribution.

In both compounds (see Table 3), dimer C displays notable contributions from both LP(N) → σ*(Te–C) interactions (3.16 kcal mol⁻¹ in **1** and 2.73 kcal mol⁻¹ in **2**) and π(CN) → σ* (Te–C) interactions (1.20 kcal mol⁻¹ in **1** and 1.45 kcal mol⁻¹ in **2**). Notably, dimer A in both compounds exhibits a minimal

Table 3 NBOs involved in the chalcogen bonding interactions and their associated second order stabilization energies ($E^{(2)}$, kcal mol⁻¹)

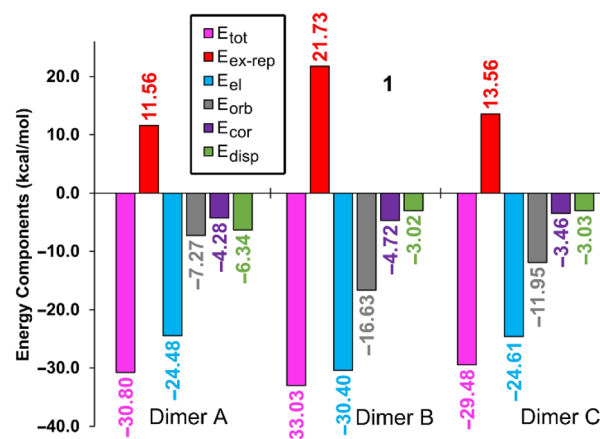| Compound	Dimer	NBOs	$E^{(2)}$
1	A	LP(N)→σ*(Te–C)	0.08
		π(CN) → σ*(Te–C)	0.74
1	B	LP(N)→σ*(Te–C)	7.76
		π(CN) → σ*(Te–C)	0.76
1	C	LP(N)→σ*(Te–C)	3.16
		π(CN) → σ*(Te–C)	1.20
2	A	LP(N) → σ*(Te–C)	0.05
		π(CN) → σ*(Te–C)	0.61
2	B	LP(N) → σ*(Te–C)	6.82
		π(CN) → σ*(Te–C)	0.58
2	C	LP(N) → σ*(Te–C)	2.73
		π(CN) → σ*(Te–C)	1.45

Fig. 7 Bar plots of the total (E_{tot}), electrostatic (E_{el}), exchange repulsion (E_{ex-rep}), orbital (E_{orb}), correlation (E_{cor}) and dispersion (E_{disp}) components of the binding energies of the chalcogen bonding assemblies of compound **1**. All values are in kcal mol⁻¹.

orbital contribution, likely attributed to the elongated Te⋯N distances and the resulting diminished orbital overlap.

For the dimer exhibiting the largest contribution within both complexes (dimer B), the associated NBOs are plotted in Fig. 6. This contribution in the EDA analysis is represented by the grey bar. Interestingly, a discernible trend emerges wherein the orbital contribution is most prominent in dimer B, followed by dimer C, and is least evident in dimer A. This pattern harmonizes effectively with the findings from the NBO analysis (Table 3).

Furthermore, the EDA calculations reveal that the underlying nature of the CAChBs is predominantly governed by electrostatics and charge transfer. Within dimers B and C, both the correlation term (E_{cor}) and the dispersion term (E_{disp}) hold similar values. In contrast, dimer A displays a larger dispersion term (E_{disp}), aligning with the establishment of an anion–π interaction where dispersion effects play a pivotal role.[63]

Conclusions

Two new telluronium salts featuring linear dicyanidoaurate anion $[Au(CN)_2]^-$ counterions have been successfully synthesized and subjected to detailed structural characterization. Given the ionic nature of these structures, the primary driving force shaping the resultant X-ray structures is the coulombic attraction. However, this work underscores the considerable influence of directional chalcogen bonds on the final assemblies.

The molecular electrostatic potential (MEP) calculations have unequivocally identified three σ-holes of comparable intensity situated at the tellurium atom. Consequently, our scrutiny of the supramolecular assemblies has focused on the formation of three distinct and directional charge-assisted chalcogen bond (CAChB) interactions facilitated by the tellurium atom. These interactions bear significant energetic implications, with compound **1** manifesting slightly heightened favourability due to the presence of the electron-withdrawing fluorine atom.

Furthermore, a comprehensive investigation of the CAChB interactions has been conducted through the combined utilization of the QTAIM and NCIPlot analyses. The NBO analysis has unveiled pivotal donor–acceptor interactions, prominently featuring electron donation from a lone pair (LP) located at the N-atom of the dicyanidoaurate anion to the vacant σ*(Te–C) antibonding orbital. The aggregate stabilization energy attributable to these charge-transfer phenomena varies markedly across different CAChB interactions, intimately tied to the Te⋯N distance.

Employing energy decomposition analysis (EDA), we have substantiated that electrostatic and charge transfer effects are preeminent within the Te⋯N contacts. The findings detailed in this study hold potential to captivate the interests of the inorganic crystal engineering and supramolecular chemistry communities, offering insights that further our comprehension of chalcogen bonding interactions.

Author contributions

S. G., A. G., E. D., R. M. G., E. P., and A. F.: investigation and data curation, A. G., E. P. and A. F.: project administration, research direction, and writing.

Conflicts of interest

There are no conflicts to declare.

Acknowledgements

References

1 Z.-L. Zhou, Y.-Z. Huang, Y. Tang, Z.-H. Chen, L.-P. Shi, X.-L. Jin and Q.-C. Yang, *Organometallics*, 1994, **13**, 1575.

2 K. J. Irgolic, *The Organic Chemistry of Tellurium*, Gordon and Breach, New York, 1974, p. 199.

3 F. Einstein, J. Trotter and C. Williston, *J. Chem. Soc. A*, 1967, 2018.

4 J.-S. Lee, D. D. Titus and R. F. Ziolo, *J. Chem. Soc., Chem. Commun.*, 1976, 501.

5 R. F. Ziolo and K. Pritchett, *J. Organomet. Chem.*, 1976, **116**, 211.

6 D. D. Titus, J.-S. Lee and R. F. Ziolo, *J. Organomet. Chem.*, 1976, **120**, 381.

7 (*a*) J.-S. Lee and D. D. Titus, *J. Cryst. Mol. Struct.*, 1976, **6**, 279; (*b*) J.-S. Lee, D. D. Titus and R. F. Ziolo, *Inorg. Chem.*, 1977, **16**, 2487.

8 E. Denes, A. Beleagă and A. Silvestru, *Inorg. Chim. Acta*, 2020, **511**, 119841.

9 P. A. Ash, J.-S. Lee, D. D. Titus, K. Bowman and R. F. Ziolo, *J. Organomet. Chem.*, 1977, **135**, 91.

10 R. V. Mitcham, B. Lee, K. B. Mertes and R. F. Ziolo, *Inorg. Chem.*, 1979, **18**, 3498.

11 R. F. Ziolo and M. Extine, *Inorg. Chem.*, 1980, **19**, 2964.

12 M. N. Ponnuswamy and J. Trotter, *Acta Crystallogr., Sect. C: Cryst. Struct. Commun.*, 1984, **40**, 1671.

13 M. J. Collins, J. A. Ripmeester and J. F. Sawyer, *J. Am. Chem. Soc.*, 1988, **110**, 8583.

14 J. Jeske, W.-W. du Mont and P. G. Jones, *Angew. Chem., Int. Ed. Engl.*, 1996, **35**, 2653.

15 (*a*) N. Sudha and H. B. Singh, *Coord. Chem. Rev.*, 1994, **135**, 469–515; (*b*) I. Haiduc, R. B. King and M. G. Newton, *Chem. Rev.*, 1994, **94**, 301–326; (*c*) E. R. T. Tiekink and J. Zuckerman-Schpector, *Coord. Chem. Rev.*, 2010, **254**, 46–76; (*d*) T. Chivers and R. S. Laitinen, *Chem. Soc. Rev.*, 2015, **44**, 1725–1739.

16 R. F. Ziolo and J. M. Troup, *Inorg. Chem.*, 1979, **18**, 2271.

17 B. H. Christian, M. J. Collins, R. J. Gillespie and J. F. Sawyer, *Inorg. Chem.*, 1986, **25**, 777.

18 G. Cavallo, P. Metrangolo, R. Milani, T. Pilati, A. Priimagi, G. Resnati and G. Terraneo, *Chem. Rev.*, 2016, **116**, 2478–2601.

19 P. Scilabra, G. Terraneo and G. Resnati, *Acc. Chem. Res.*, 2019, **52**, 1313–1324.

20 S. Scheiner, *Acc. Chem. Res.*, 2013, **46**, 280–288.

21 A. Bauzá, T. J. Mooibroek and A. Frontera, *Angew. Chem., Int. Ed.*, 2013, **52**, 12317–12321.

22 A. Bauzá and A. Frontera, *Angew. Chem., Int. Ed.*, 2015, **54**, 7340–7343.

23 S. Grabowski, *J. Comput. Chem.*, 2018, **39**, 472–480.

24 (*a*) P. Politzer and J. S. Murray, *Crystals*, 2017, **7**, 212–226; (*b*) I. Alkorta, J. Elguero and A. Frontera, *Crystals*, 2020, **10**, 180; (*c*) J. S. Murray, P. Lane, T. Clark, K. E. Riley and P. Politzer, *J. Mol. Model.*, 2012, **18**, 541–548.

25 B. Mallada, A. Gallardo, M. Lamanec, B. de la Torre, V. Špirko, P. Hobza and P. Jelinek, *Science*, 2021, **374**, 863–867.

26 G. Cavallo, P. Metrangolo, T. Pilati, G. Resnati and G. Terraneo, *Cryst. Growth Des.*, 2014, **14**, 2697–2702.

27 A. Bauzá, T. J. Mooibroek and A. Frontera, *ChemPhysChem*, 2015, **16**, 2496–2517.

28 C. B. Aakeroy, D. L. Bryce, G. R. Desiraju, A. Frontera, A. C. Legon, F. Nicotra, K. Rissanen, S. Scheiner, G. Terraneo, P. Metrangolo and G. Resnati, *Pure Appl. Chem.*, 2019, **91**, 1889–1892.

29 (*a*) J. Y. C. Lim and P. D. Beer, *Chem*, 2018, **4**, 731–783; (*b*) P. Scilabra, G. Terraneo and G. Resnati, *J. Fluorine Chem.*, 2017, **203**, 62–74.

30 (*a*) D. J. Pascoe, K. B. Ling and S. L. Cockroft, *J. Am. Chem. Soc.*, 2017, **139**, 15160–15167; (*b*) S. Scheiner, *Chem. – Eur. J.*, 2016, **22**, 18850–18858.

31 E. Alikhani, F. Fuster, B. Madebene and S. J. Grabowski, *Phys. Chem. Chem. Phys.*, 2014, **16**, 2430–2442.

32 W. Wang, H. Zhu, S. Liu, Z. Zhao, L. Zhang, J. Hao and Y. Wang, *J. Am. Chem. Soc.*, 2019, **141**, 9175–9179.

33 M. Macchione, A. Goujon, K. Strakova, H. V. Humeniuk, G. Licari, E. Tajkhorshid, N. Sakai and S. Matile, *Angew. Chem., Int. Ed.*, 2019, **58**, 15752–15756.

34 K. Strakova, L. Assies, A. Goujon, F. Piazzolla, H. V. Humeniuk and S. Matile, *Chem. Rev.*, 2019, **119**, 10977–11005.

35 K. T. Mahmudov, M. N. Kopylovich, M. F. C. Guedes da Silva and A. J. L. Pombeiro, *Dalton Trans.*, 2017, **46**, 10121–10138.

36 B. Galmés, A. Juan-Bals, A. Frontera and G. Resnati, *Chem. – Eur. J.*, 2020, **26**, 4599–4606.

37 U. Adhikari and S. Scheiner, *J. Phys. Chem. A*, 2014, **118**, 3183–3192.

38 S. Scheiner, *J. Phys. Chem. A*, 2015, **119**, 9189–9199.

39 R. Oilunkaniemi, J. Pietikainen, R. S. Laitinen and M. Ahlgren, *J. Organomet. Chem.*, 2001, **640**, 50.

40 K. Swaminathan, P. J. Carroll, Kochurani, H. B. Singh and H. D. Bhargava, *Acta Crystallogr., Sect. C: Cryst. Struct. Commun.*, 1993, **49**, 1243.

41 R. F. W. Bader, *Chem. Rev.*, 1991, **91**, 893–928.

42 E. R. Johnson, S. Keinan, P. Mori-Sánchez, J. Contreras-García, A. J. Cohen and W. Yang, *J. Am. Chem. Soc.*, 2010, **132**, 6498–6506.

43 E. D. Glendening, C. R. Landis and F. Weinhold, *Wiley Interdiscip. Rev.: Comput. Mol. Sci.*, 2012, **2**, 1–42.

44 K. Kitaura and K. Morokuma, *Int. J. Quantum Chem.*, 1976, **10**, 325–340.

45 R. Ahlrichs, M. Bär, M. Hacer, H. Horn and C. Kömel, *Chem. Phys. Lett.*, 1989, **162**, 165–169.

46 C. Adamo and V. Barone, *J. Chem. Phys.*, 1999, **110**, 6158–6170.

47 E. Caldeweyher, S. Ehlert, A. Hansen, H. Neugebauer, S. Spicher, C. Bannwarth and S. Grimme, *J. Chem. Phys.*, 2019, **150**, 154122.

48 F. Weigend, *Phys. Chem. Chem. Phys.*, 2006, **8**, 1057–1065.

49 D. Andrae, U. Haeussermann, M. Dolg, H. Stoll and H. Preuss, *Theor. Chim. Acta*, 1990, **77**, 123–141.

50 T. Lu and F. Chen, *J. Comput. Chem.*, 2012, **33**, 580–592.

51 J. W. Humphrey, A. Dalke and K. Schulten, *J. Mol. Graphics*, 1996, **14**, 33–38.

52 R. Dennington, T. A. Keith and J. M. Millam, *GaussView, Version 6.1*, Semichem Inc., Shawnee Mission, KS, 2019.

53 E. D. Glendening, J. K. Badenhoop, A. E. Reed, J. E. Carpenter, J. A. Bohmann, C. M. Morales, P. Karafiloglou, C. R. Landis and F. Weinhold, *NBO 7.0*, Theoretical Chemistry Institute, University of Wisconsin, Madison, WI, USA, 2018.

54 T. M. Klapotke, B. Krumm, P. Mayer, H. Piotrowski, I. Schwab and M. Vogt, *Eur. J. Inorg. Chem.*, 2002, 2701–2709.

55 (*a*) E. Priola, G. Volpi, R. Rabezzana, E. Borfecchia, C. Garino, P. Benzi, A. Martini, L. Operti and E. Diana, *Inorg. Chem.*, 2020, **59**, 203–213; (*b*) A. Giordana, R. M. Gomila, R. Rabezzana, E. Laurenti, E. Priola, B. Eftekhar-Sis, G. Mahmoudi and A. Frontera, *ChemPlusChem*, 2023, **88**, e202300052.

56 M. C. Aragoni, M. Arca, V. Lippolis, A. Pintus, Y. Torubaev and E. Podda, *Molecules*, 2023, **28**, 3133.

57 (*a*) E. Priola, A. Giordana, P. P. Mazzeo, G. Mahmoudi, R. M. Gomila, F. I. Zubkov, K. M. Pokazeev, K. S. Valchuk, A. Bacchi, E. Zangrando and A. Frontera, *Dalton Trans.*, 2021, **50**, 16954–16960; (*b*) E. Priola, N. Curetti,

D. Marabello, J. Andreo, A. Giordana, L. Andreo, P. Benna, P. T. C. Freire, P. Benzi, L. Operti and E. Diana, *CrystEngComm*, 2022, **24**, 2336–2348.

58 N. S. Dance, W. R. McWhinnie, J. Mallaki and Z. Monsef-Mirzai, *J. Organomet. Chem.*, 1980, **198**, 131–143.

59 N. S. Dance and W. R. McWhinnie, *J. Chem. Soc., Dalton Trans.*, 1975, 43–45.

60 D. H. Whiffen, *J. Chem. Soc.*, 1956, 1350–1356.

61 B. M. Chadwick and S. G. Frankiss, *J. Mol. Struct.*, 1976, **31**, 1–9.

62 (*a*) S. Kolb, G. A. Oliver and D. B. Werz, Chalcogen bonding in supramolecular structures, anion recognition, and catalysis, in *Comprehensive Inorganic Chemistry III*, ed. R. S. Laitinen, Elsevier, Oxford, 2023, vol. 1, pp. 602–651; (*b*) S. Kolb, G. A. Oliver and D. B. Werz, *Angew. Chem., Int. Ed.*, 2020, **59**, 22306–22310; (*c*) R. Gleiter, G. Haberhauer, D. B. Werz, F. Rominger and C. Bleiholde, *Chem. Rev.*, 2018, **118**, 2010–2041; T. Chivers and R. S. Laitinen, *Chem. Soc. Rev.*, 2015, **44**, 1725–1739; A. F. Cozzolino, P. J. W. Elder and I. Vargas-Baca, *Coord. Chem. Rev.*, 2011, **255**, 1426–1438.

63 (*a*) A. Frontera, P. Gamez, M. Mascal, T. J. Mooibroek and J. Reedijk, *Angew. Chem., Int. Ed.*, 2011, **50**, 9564–9583; (*b*) D. Quiñonero, C. Garau, C. Rotger, A. Frontera, P. Ballester, A. Costa and P. M. Deyà, *Angew. Chem., Int. Ed.*, 2002, **41**, 3539–3542.